Efficient flexible organic photovoltaics using silver nanowires and polymer based transparent electrodes

Yoonseok Park [a, *], Ludwig Bormann [a], Lars Müller-Meskamp [a], Koen Vandewal [a], Karl Leo [a, b, **]

[a] Institut für Angewandte Photophysik, George-Bähr-Strasse 1, 01062, Dresden, Germany
[b] Fellow of the Canadian Institute for Advanced Research (CIFAR), Canada

ARTICLE INFO

ABSTRACT

Planarization and filling voids between wires are key issues when using nanowire electrodes in flexible solar cells such as organic photovoltaics (OPV). For this purpose, we use poly(3,4-ethylenedioxythiophene):poly(styrenesulfonate) (PEDOT: PSS) which leads to an electrically well connected silver nanowire (AgNW) network. Furthermore, the use of water based PEDOT: PSS leads to humidity assisted AgNW fusing, resulting in a maximum processing temperature of only 120 °C. OPV cells using this AgNW/PEDOT: PSS transparent electrodes exhibit power conversion efficiencies up to 7.15%. Moreover, OPV devices on PET substrates with an alumina encapsulation and barrier adhesive show excellent mechanical flexibility.

© 2016 Elsevier B.V. All rights reserved.

1. Introduction

Small molecule organic photovoltaics (OPV) are prospective candidates for future renewable energy production because of their potential scalability, low cost, and flexibility. For establishing flexible organic devices, a highly transparent, conductive and flexible electrode is required, replacing indium tin oxide (ITO) which is brittle and requires high temperature processes. Many alternative materials such as conductive polymers [1–3], graphene [4], carbon nanotubes [5–7], thin metal [8–10] and metal nanowires [11–13] have been studied. Among these, metal nanowires, especially silver nanowire (AgNW) networks, show outstanding flexibility, conductivity, and transparency [14,15]. However, AgNW network electrodes have a few structural innate problems. First, after deposition of the AgNW network, there is a poor electrical contact between wires, resulting in a low conductivity. Secondly, overlapping wires cause roughness, often resulting in electrical shorting of devices deposited on top of these electrodes. To create a smooth and well connected network, post-treatment techniques such as mechanical pressure [16], plasmonic welding [17,18], thermal treatment [12], and humidity assisted low temperature treatments [19] have been applied. Thirdly, open spaces between wires can be in the range of square micrometers. Charge carriers photo-generated in the absorber layer within such a void might not be able to reach the highly conductive network and get lost due to recombination. To overcome this, the nanowire network [20] can be coated by a solution—processed hole transport layer, planarizing the nanowire network. Both low conductive PEDOT: PSS [21] and high conductive PEDOT: PSS [12] have been deposited on AgNW electrodes to form conductive bridges between open spaces and to smoothen the sharp points of the network. The required annealing temperature of 180 °C is incompatible with low-cost flexible PET substrates. A low temperature process (60 °C) employing two-step spray-coated silver nanowires and PEDOT: PSS has been reported [22]. However, this process results in shunts in the organic photovoltaic device and a low (25%) fill factors. Moreover, residual water in the PEDOT: PSS could still be present due to the low annealing temperature (60 °C), affecting the device stability.

In this work, Spray-coated AgNW electrodes with thin PEDOT: PSS are prepared on glass and PET substrates and maximum 120 °C process is done during preparation (PET is stable at 120 °C but over

* Corresponding author.
** Corresponding author.
E-mail addresses: yoonseok.park@iapp.de (Y. Park), karl.leo@iapp.de (K. Leo).

140 °C it shrinks). A sheet resistance (R_S) of 30 $\Omega/\square$ and a total transmittance of 86% are achieved for both NW35 and NW90. This performance is comparable to a NW90 electrode with 85% total transmittance and R_S of 28.6 $\Omega/\square$ [19] and significantly better than that of a 120 nm PEDOT: PSS electrode, which has an Rs of 100 $\Omega/\square$, insufficient for large size devices. OPV devices were deposited on these electrodes with glass and PET substrates. The power conversion efficiency of OPV devices on glass with AgNW and ITO are 7.15% and 7.92%, respectively. Moreover, flexible devices on a PET substrate achieve a PCE of 6.91%.

2. Results and discussion

AgNW electrodes combined with PEDOT: PSS (total transmittance: 86%, R_S: 30 $\Omega/\square$) are prepared, using less Ag than for neat AgNW electrodes [19] (total transmittance: 85%, R_S: 28.6 $\Omega/\square$) by reducing the number of AgNW sprayed in our setup. For making AgNW/PEDOT: PSS electrode, AgNW networks on substrates with 90% transmittance are prepared; for these layers, the Rs is too high to be measured in our setup. However, by subsequently spin-coating 40 nm of PEDOT: PSS (600 $\Omega/\square$) and an annealing at 120 °C for 15 min, the R_S decreases to less than 30 $\Omega/\square$, with the total transmittance decreasing to 86%. To check whether the electrical enhancement primarily comes from the conductivity of PEDOT: PSS or the formation of AgNW networks by annealing, R_S is measured after 5 min, which is too short for forming the network between wires. In this case, R_S is higher than 500 $\Omega/\square$ as shown in Fig. 1. This result indicates the conductivity of the AgNW electrode is mainly improved by electrical connections between AgNWs and only slightly improved by the conductivity of PEDOT: PSS.

AFM images in Fig. 2(a) and (c) show the morphology of the AgNW network with and without the additional PEDOT: PSS layer after 15 min annealing on a 120 °C hotplate. Although three nanowires overlap in Fig. 2(c), the highest point is 142 nm which is less than the sum of three nanowires of 90 nm diameter. Without the use of PEDOT: PSS, the overall roughness is significantly larger (Fig. 2(a)). This shows that PEDOT: PSS helps fusing the nanowires. AgNW electrodes with and without PEDOT: PSS on glass with one corner contacted by silver paste are measured by Conductive AFM (c-AFM). The resulting current maps with the applied bias voltage

of 1 V are shown in the inset of Fig. 2(b), No current could be detected by c-AFM for nanowires without PEDOT: PSS (Fig. 2(b)). On the other hand, a uniformly distributed current is measured for the AgNW network embedded in PEDOT: PSS. The AgNW shape still appears in the c-AFM image, as marked with arrows in Fig. 2(d). Lower conductivity spots are observed on the left side of wires, which is an artifact of the direction of measurement. Scanning electron microscopy (SEM) is used to compare the topography of the electrodes. AgNW annealed at 120 °C without PEDOT: PSS do not show a fused, interconnecting network of wires. Moreover, the surfactant polyvinylpyrrolidone (PVP), used as stabilizer for silver nanowires synthesis, is still observed around the AgNW (Fig. 3(a) and (b)). After coverage of the AgNW by PEDOT: PSS deposition, it is impossible to observe whether PVP is still present. However, we expect that the water-soluble PVP has been partly washed off, improving the connection between the wires. Fig. 3(c) and (d) show that the network is smoothened upon PEDOT: PSS deposition. These results indicate that PEDOT: PSS deposition helps connecting the AgNW network by filling the voids between the AgNWs, by fusing the junctions, and softening the rough and sharp spots. The possible reasons why AgNWs are fusing at relatively low temperature are (i) a softening of the wet PVP shell, which allows an elastic alignment of the NWs and thereby enhancing electrical contact between wires as mentioned by Weiß et al. [19]. (ii) A removal of PVP from the AgNWs during PEDOT: PSS processing might open free paths for a surface diffusion of silver atoms and the formation of joints between wires as explained by Zhu et al. [23].

The electrode performance of the AgNW network is evaluated in OPV devices using a DCV5T-Me:C_{60} bulk heterojunction absorber layer. The photovoltaic device is deposited on top of AgNW electrodes with and without PEDOT: PSS on both a glass and PET substrates. A reference device containing an ITO electrode was fabricated in parallel. The AgNW electrode without PEDOT: PSS yields short-circuited devices for both NW35 and NW90. However, when using a PEDOT: PSS smoothed AgNW electrode, the shunt resistance (24.8 kΩ for NW30, 25.5 kΩ for NW90) is comparable to that of a device on ITO (26.4 kΩ) as shown in Table 1. As shown in Fig. 4 and 7.15% of power conversion efficiency (PCE) with a short-circuit current density (J_{sc}) of 12.34 mA/cm^2, open circuit voltage (V_{oc}) of 0.955 V, and a fill factor (FF) of 60.67% are achieved by the device using a NW90 electrode with PEDOT: PSS. Even if this value is not as high as OPV using ITO electrode (7.92%), it is the best performance published up to now using small molecule OPV on AgNW electrode, to best of our knowledge. The reason why OPVs using ITO electrodes still show higher performance than OPVs using AgNW electrodes is that the direct reflectance of AgNW electrode is lower than that of ITO as shown in Fig. 1 and the low direct reflection does not support a microcavity effect [24] as discussed in a previous study [25].

The NW35 electrode with PEDOT: PSS is also tested in OPV devices. With 30 $\Omega/\square$, the electrical performance of NW35 and NW90 electrodes is very similar. However, J_{sc} shows 11.57 mA/cm^2 which is 7% less as compared to NW90. As shown in Fig. 1, NW35 electrodes exhibit a stronger plasmonic dip around a wavelength of 350 nm and lower transmittance from 600 nm to 800 nm as compared to NW90 explaining the reduced J_{sc}.

Using PET as substrate, we further demonstrate a fully flexible, encapsulated OPV device. The device is protected by a flexible 20 nm AlO$_x$ (Water vapor transmission rate of 2 × 10^{-5} g/m^2 day) thin-film encapsulation [26]. A maximum PCE of 6.91% is achieved; the degradation of OPVs with this encapsulation has been investigated by Bormann et al. [27]. For checking the electrical stability of AgNW/PEDOT: PSS as electrode for flexible devices, a bending test is performed in ambient condition. The performance of devices is stable over 20 cycles of bending with 3 mm radius as shown in
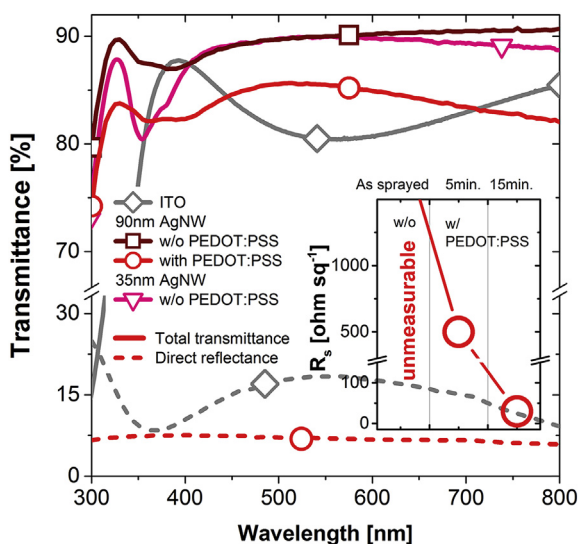
Fig. 1. Total transmittance and direct reflectance of silver nanowires network with and without PEDOT: PSS. The inset shows sheet resistance before PEDOT: PSS coating and after PEDOT: PSS depending on the annealing time.
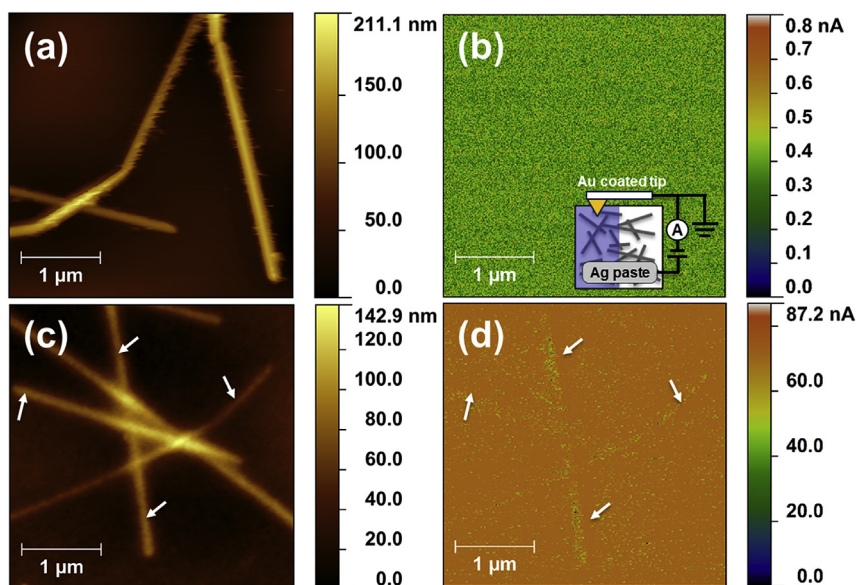
Fig. 2. AFM (left) and conductive AFM (right) images of silver nanowires network (NW90) without PEDOT: PSS (a), (b) and with PEDOT: PSS (c), (d).
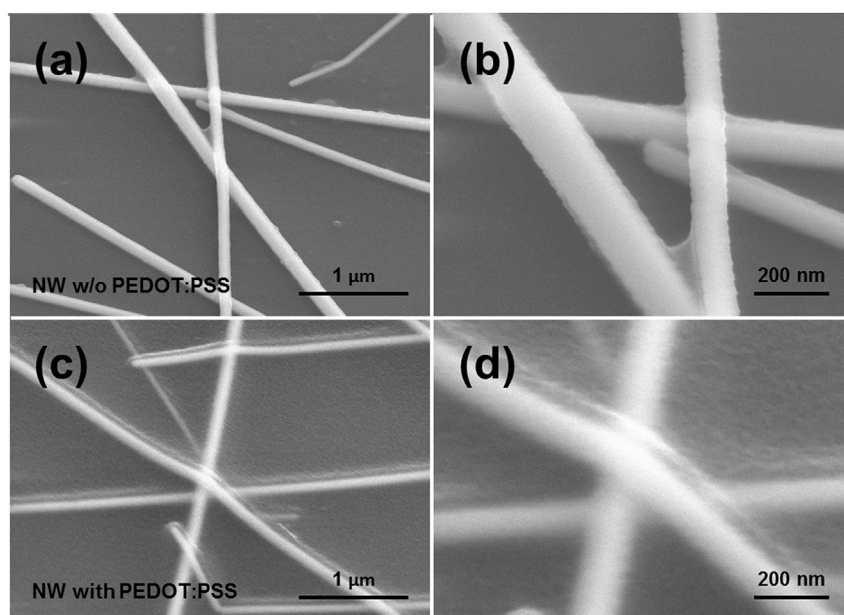

Fig. 3. SEM images of silver nanowires network without PEDOT: PSS (a), (b) and with PEODT: PSS (c), (d).

Table 1
OPV device performance parameters for nanowires electrodes on glass and PET substrates and ITO on glass substrates.

	J_{sc} [mA/cm^2]	V_{oc} [V]	FF [%]	PCE [%]	R_{sh} [kΩ]
NW90 on glass	12.34 (±0.1)	0.955	60.67 (±0.1)	7.15 (±0.1)	25.5 (±0.2)
NW90 on PET	12.31 (±0.1)	0.938	58.42 (±0.1)	6.91 (±0.1)	16.9 (±0.3)
NW35 on glass	11.57 (±0.6)	0.944	63.07 (±0.1)	6.93 (±0.3)	24.8 (±1.2)
ITO on glass	13.74 (±0.1)	0.951	60.65 (±0.1)	7.92 (±0.0)	26.4 (±0.2)

Fig. 5. This result proves the good bending stability of AgNW electrodes when used in an OPV device.

In summary, OPV devices using ITO-free AgNW-PEDOT: PSS hybrid electrodes show a PCE of 7.15% which is the best performance of small molecule OPV using AgNW electrodes so far. By depositing the PEDOT: PSS layer, the voids in the AgNW network are filled and the rough and sharp AgNW surface is sufficiently smoothened for use within an OPV device. Moreover, Ag (one third of other studies) can be spared and an extra, high temperature annealing process for a good electrical connection between the nanowires can be avoided. OPV devices are demonstrated on PET substrates with a flexible AgNW electrode, showing a largely retained performance when bent at radii down to 3 mm.

3. Experimental

ITO coated glass and BK7 glass of 2.5 × 2.5 cm^2 (Schott, Mainz, Germany) and polyethylene terephthalate (PET) foil (Melinex ST504, DuPont Teijin Films) are rinsed with isopropanol and water, subsequently treated with oxygen plasma 2 × 10^{-1} mbar, 10 min.
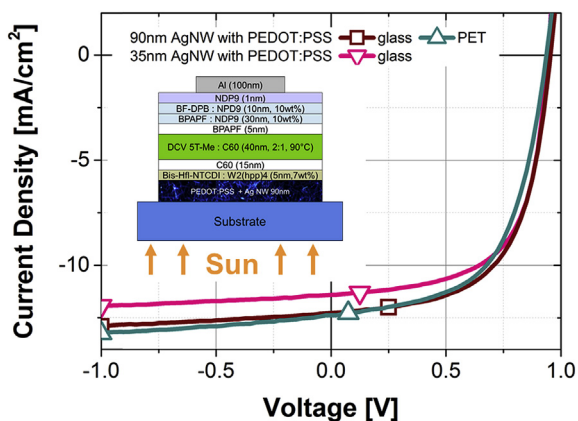
Fig. 4. J-V curves of OPV devices on silver nanowires and PEDOT: PSS electrode with a scheme of the OPV device architecture.
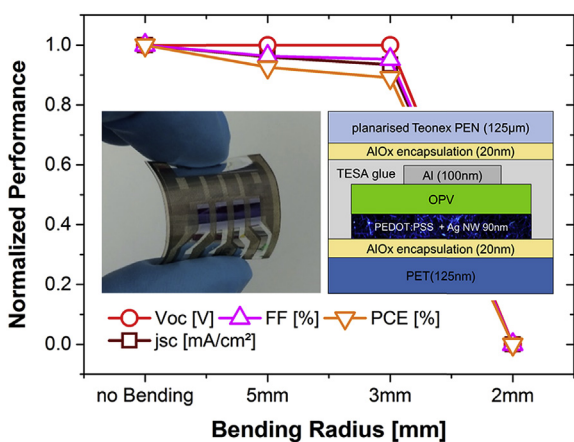

Fig. 5. Normalized performance parameters of OPV device after bending. Performance is measured after 20 cycles of bending with radius of 5, 3 and 2 mm.

Silver nanowires SLV-NW-90 and SLV-NW-35 (mean diameter 90 nm and 35 nm, BlueNano, USA) are diluted with ethanol to a concentration of 0.2 mg/ml, sonicated for 15 min and then spray-coated with a nozzle (Fisnar, Wayne (NJ), USA) onto a heated substrate at 80 °C. The spraying distance, moving speed and spraying pressure of the nozzle were 12 cm, 1.5 cm/s and 200 mbar, respectively. To achieve sufficient electrical property, highly conductive PEDOT: PSS (Clevios PH1000, Heraeus, Germany) solution is mixed with 6 vol % ethylene glycol and spun on top of the nanowires (2500 rpm, 30 s), followed by a curing step at 120 °C for 15 min to remove residual water in the layers [28]. After coating of the substrates with the electrodes, a Nd:YAG laser marking system (ACI Laser GmbH, Germany) is used for patterning the bottom electrodes to avoid cross-talk between pixels during current-voltage measurements. Electrodes are optically characterized with a Shimadzu MPC3100 Spectrophotometer with Ulbricht sphere. AFM (AIST-NT Combiscope, USA) is used to characterize the surface morphology and local conductivity. A Carl Zeiss DSM 982 scanning electron microscopy is used for acquiring SEM images. Sheet resistance is measured using a four point probe setup (Lucas Labs, USA).

Small molecule OPV devices are fabricated by thermal evaporation in a vacuum chamber (K. J. Lesker, U. K.) at a base pressure of around 10^{-8} mbar, as described previously [29]. The cell stack consists of a 5 nm *N,N*-Bis(*fluoren-2-yl*)-naphthalenetetracarboxylic diimide (Bis-Hfl-NTCDI) transparent matrix material, doped by 7 wt % of tetrakis(1,3,4,6,7,8-hexahydro-2H-pyrimido [1,2-a]pyrimidinato)ditungsten (II) (W$_2$(hpp)4)/ 15 nm C$_{60}$ fullerene as electron transport layer/40 nm of mixed DCV5T-Me and fullerene C$_{60}$ (ratio of 2:1) as an absorber layer/5 nm 9,9-bis[4–(*N,N*-bis-biphenyl-4-yl-amino)phenyl]-9H-fluorene (BPAPF) as hole transporting layer/30 nm of BPAPF and 10 nm of N,N′-((Diphenyl-N,N′-bis)9,9,-dimethyl-fluoren-2-yl)-benzidine (BF-DPB) transparent matrix materials doped with 10 wt % NDP9 (Novaled AG) and finally a 100 nm Al cathode. For preparing the bottom encapsulation for OPV on PET substrate, a 20 nm thick AlO$_x$ thin film is deposited by plasma enhanced ALD in a Sentech SI reactor (SENTECH Instruments GmbH, Berlin, Germany) on PET substrates. At 100 °C electrode temperature, 220 cycles are done using electronic grade trimethylaluminium (TMA) and atomic oxygen from the plasma as precursors. In between precursor pulses, the chamber is purged with 99.9999% chemical purity nitrogen gas. For the top encapsulation, an equivalent thin-film is deposited on 125 μm planarised Teonex PEN (Dupont Teijin Films Ltd.,UK). In a glovebox, this barrier film is directly laminated onto the OPV devices using a barrier adhesive film (tesa SE, Germany) [27,30], which contains a latent getter against lateral oxygen and water diffusion. Current voltage measurements are measured by using a source measurement unit 2400 SMU (Keithley, USA) and simulated AM 1.5G sun light (16S–150 V.3 by Solar Light Co., USA) taking spectral mismatch into account. The illumination intensity is kept at (100 ± 1) mW/cm^2 monitored by a silicon reference diode. The EQE used to calculate the mismatch factor was measured using a lock-in amplifier (Signal Recovery SR 7265) with the device under monochromatic illumination (Oriel Xe Arc-Lamp Apex Illuminator combined with Cornerstone 260 1/4 m monochromator, Newport, USA).

Acknowledgements

References

[1] Y. Hyun Kim, C. Sachse, M. Hermenau, K. Fehse, M. Riede, L. Muller-Meskamp, et al., Improved efficiency and lifetime in small molecule organic solar cells with optimized conductive polymer electrodes, Appl. Phys. Lett. 99 (2011) 113305, http://dx.doi.org/10.1063/1.3634015.

[2] F. Zhang, M. Johansson, M.R. Andersson, J.C. Hummelen, O. Inganäs, Polymer photovoltaic cells with conducting polymer anodes, Adv. Mater. 14 (2002) 662–665, http://dx.doi.org/10.1002/1521-4095(20020503)14, 9<662::AID-ADMA662>3.0.CO;2-N.

[3] S.-I. Na, S.-S. Kim, J. Jo, D.-Y. Kim, Efficient and flexible ITO-free organic solar cells using highly conductive polymer anodes, Adv. Mater. 20 (2008) 4061–4067, http://dx.doi.org/10.1002/adma.200800338.

[4] S. Bae, H. Kim, Y. Lee, X. Xu, J.-S. Park, Y. Zheng, et al., Roll-to-roll production of 30-inch graphene films for transparent electrodes, Nat. Nanotechnol. 5 (2010) 574–578, http://dx.doi.org/10.1038/nnano.2010.132.

[5] M.W. Rowell, M.A. Topinka, M.D. McGehee, H.-J. Prall, G. Dennler, N.S. Sariciftci, et al., Organic solar cells with carbon nanotube network electrodes, Appl. Phys. Lett. 88 (2006) 233506, http://dx.doi.org/10.1063/1.2209887.

[6] D.-J. Yun, J.-M. Kim, H. Ra, S. Byun, H. Kim, G.-S. Park, et al., The physical/chemical properties and electrode performance variations of SWNT films in consequence of solution based surfactant elimination processes, Org. Electron. 14 (2013) 2962–2972, http://dx.doi.org/10.1016/j.orgel.2013.08.021.

[7] Y.H. Kim, C. Sachse, A. a Zakhidov, J. Meiss, A. a Zakhidov, L. Müller-Meskamp, et al., Combined alternative electrodes for semi-transparent and ITO-free

small molecule organic solar cells, Org. Electron. 13 (2012) 2422–2428, http://dx.doi.org/10.1016/j.orgel.2012.06.034.

[8] S. Schubert, J. Meiss, L. Müller-Meskamp, K. Leo, Improvement of transparent metal top electrodes for organic solar cells by introducing a high surface energy seed layer, Adv. Energy Mater. 3 (2013) 438–443, http://dx.doi.org/10.1002/aenm.201200903.

[9] S. Schubert, M. Hermenau, J. Meiss, L. Müller-Meskamp, K. Leo, Oxide sandwiched metal thin-film electrodes for long-term stable organic solar cells, Adv. Funct. Mater. 22 (2012) 4993–4999, http://dx.doi.org/10.1002/adfm.201201592.

[10] D.S. Ghosh, Q. Liu, P. Mantilla-Perez, T.L. Chen, V. Mkhitaryan, M. Huang, et al., Highly flexible transparent electrodes containing ultrathin silver for efficient polymer solar cells, Adv. Funct. Mater. 25 (2015) 7309–7316, http://dx.doi.org/10.1002/adfm.201503739.

[11] W. Gaynor, G.F. Burkhard, M.D. McGehee, P. Peumans, Smooth nanowire/polymer composite transparent electrodes, Adv. Mater. 23 (2011) 2905–2910, http://dx.doi.org/10.1002/adma.201100566.

[12] C. Sachse, L. Müller-Meskamp, L. Bormann, Y.H. Kim, F. Lehnert, A. Philipp, et al., Transparent, dip-coated silver nanowire electrodes for small molecule organic solar cells, Org. Electron. 14 (2013) 143–148, http://dx.doi.org/10.1016/j.orgel.2012.09.032.

[13] F. Selzer, N. Weiß, D. Kneppe, L. Bormann, C. Sachse, N. Gaponik, et al., A spray-coating process for highly conductive silver nanowire networks as the transparent top-electrode for small molecule organic photovoltaics, Nanoscale 7 (2015) 2777–2783, http://dx.doi.org/10.1039/C4NR06502F.

[14] L. Hu, H.S. Kim, J.-Y. Lee, P. Peumans, Y. Cui, Scalable coating and properties of transparent, flexible, silver nanowire electrodes, ACS Nano 4 (2010) 2955–2963, http://dx.doi.org/10.1021/nn1005232.

[15] Z. Yu, Q. Zhang, L. Li, Q. Chen, X. Niu, J. Liu, et al., Highly flexible silver nanowire electrodes for shape-memory polymer light-emitting diodes, Adv. Mater. 23 (2011) 664–668, http://dx.doi.org/10.1002/adma.201003398.

[16] S.-E. Park, S. Kim, D.-Y. Lee, E. Kim, J. Hwang, S.I. Na, et al., Fabrication of silver nanowire transparent electrodes using electrohydrodynamic spray deposition for flexible organic solar cells, J. Mater. Chem. A 1 (2013) 14286, http://dx.doi.org/10.1039/c3ta13204h.

[17] E.C. Garnett, W. Cai, J.J. Cha, F. Mahmood, S.T. Connor, M. Greyson Christoforo, et al., Self-limited plasmonic welding of silver nanowire junctions, Nat. Mater. 11 (2012) 241–249, http://dx.doi.org/10.1038/nmat3238.

[18] T. Tokuno, M. Nogi, M. Karakawa, J. Jiu, T.T. Nge, Y. Aso, et al., Fabrication of silver nanowire transparent electrodes at room temperature, Nano Res. 4 (2011) 1215–1222, http://dx.doi.org/10.1007/s12274-011-0172-3.

[19] N. Weiß, L. Mueller-Meskamp, F. Selzer, L. Bormann, A. Eychmueller, K. Leo, et al., Humidity assisted annealing technique for transparent conductive silver nanowires networks, RSC Adv. 5 (2015) 19659–19665, http://dx.doi.org/10.1039/C5RA01303H.

[20] L. Bormann, F. Selzer, N. Weiß, D. Kneppe, K. Leo, L. Müller-Meskamp, Doped hole transport layers processed from solution: planarization and bridging the voids in noncontinuous silver nanowire electrodes, Org. Electron. Phys. Mater. Appl. 28 (2016) 163–171, http://dx.doi.org/10.1016/j.orgel.2015.10.007.

[21] M. Song, D.S. You, K. Lim, S. Park, S. Jung, C.S. Kim, et al., Highly efficient and bendable organic solar cells with solution-processed silver nanowire electrodes, Adv. Funct. Mater. 23 (2013) 4177–4184, http://dx.doi.org/10.1002/adfm.201202646.

[22] D.Y. Choi, H.W. Kang, H.J. Sung, S.S. Kim, Annealing-free, flexible silver nanowire-polymer composite electrodes via a continuous two-step spray-coating method, Nanoscale 5 (2013) 977–983, http://dx.doi.org/10.1039/c2nr32221h.

[23] S. Zhu, Y. Gao, B. Hu, J. Li, J. Su, Z. Fan, et al., Transferable self-welding silver nanowire network as high performance transparent flexible electrode, Nanotechnology 24 (2013) 335202, http://dx.doi.org/10.1088/0957-4484/24/33/335202.

[24] H.-W. Lin, S.-W. Chiu, L.-Y. Lin, Z.-Y. Hung, Y.-H. Chen, F. Lin, et al., Device engineering for highly efficient top-illuminated organic solar cells with microcavity structures, Adv. Mater. 24 (2012) 2269–2272, http://dx.doi.org/10.1002/adma.201200487.

[25] L. Bormann, F. Nehm, L. Sonntag, F.-Y. Chen, F. Selzer, L. Mueller-Meskamp, et al., Degradation of Flexible, ITO-free Oligothiophene Organic Solar Cells, ACS Appl. Mater. Interfaces. 8 (2016) 14709–14716, http://dx.doi.org/10.1021/acsami.6b02363.

[26] F. Nehm, H. Klumbies, C. Richter, A. Singh, U. Schroeder, T. Mikolajick, et al., Breakdown and protection of ALD moisture barrier thin films, ACS Appl. Mater. Interfaces 7 (2015) 22121–22127, http://dx.doi.org/10.1021/acsami.5b06891.

[27] L. Bormann, F. Nehm, N. Weiß, V.C. Nikolis, F. Selzer, A. Eychmüller, et al., Degradation of sexithiophene cascade organic solar cells, Adv. Energy Mater. (2016), http://dx.doi.org/10.1002/aenm.201502432 n/a–n/a.

[28] Y.H. Kim, C. Sachse, M.L. Machala, C. May, L. Müller-Meskamp, K. Leo, Highly conductive PEDOT: PSS electrode with optimized solvent and thermal post-treatment for ITO-free organic solar cells, Adv. Funct. Mater. 21 (2011) 1076–1081, http://dx.doi.org/10.1002/adfm.201002290.

[29] R. Meerheim, C. Körner, K. Leo, Highly efficient organic multi-junction solar cells with a thiophene based donor material, Appl. Phys. Lett. 105 (2014) 063306, http://dx.doi.org/10.1063/1.4893012.

[30] Y. Park, F. Nehm, L. Müller-Meskamp, K. Vandewal, K. Leo, Optical display film as flexible and light trapping substrate for organic photovoltaics, Opt. Express 24 (2016) A974, http://dx.doi.org/10.1364/OE.24.00A974.